Consequences of electronic-state mixing on the dynamics of photodissociation of H_2 by barrier tunneling

Laurens D. A. Siebbeles, Juleon M. Schins, and Wim J. van der Zande
FOM—Institute for Atomic and Molecular Physics, Kruislaan 407, 1098 SJ Amsterdam, The Netherlands

J. Alberto Beswick
Laboratoire pour l'Utilisation du Rayonnement Electromagnétique, Université de Paris–Sud, 91405 Orsay, France

Nadine Halberstadt
Laboratoire Photophysique Moleculaire, Université de Paris–Sud, 91405 Orsay, France
(Received 20 November 1991)

The effect of electronic state mixing on tunneling dynamics is studied. To this aim the theoretical description of the differential photodissociation cross section is extended to include rotational and vibrational couplings. The mixing of bound and quasibound electronic states is reflected in resonance widths. The anisotropy of the photofragments reflects mixing of dissociative continua. It is shown that inclusion of these nonadiabatic couplings is required to reproduce the recently reported [Siebbeles, Schins, Los, and Glass-Maujean, Phys. Rev. A **44**, 343 (1991)] differential photodissociation cross section of H_2 for excitation around the $e\,^3\Pi_g$ ($v'=5$, $N'=1,2$) resonances. Nonclassical photofragment anisotropies are found for coherent excitation of different rotational resonances ($v'=5$, $N'=1$, and $N'=2$) and of different rovibrational resonances ($v'=5$, $N'=1$ and $v'=4$, $N'=2$). The latter is strongly connected to the molecular excitation mechanism and has therefore no parallel in collision experiments.

PACS number(s): 33.80.Gj, 33.10.Lb, 35.20.Jv, 35.20.Pa

I. INTRODUCTION

Recently [1] we reported on the differential cross section for photodissociation of H_2 by tunneling through the barrier in the electronic potential of the $e\,^3\Pi_g$ state; see Fig. 1. The experimental and calculated cross sections in Ref. [1] exhibit discrepancies. The calculated cross sections and anisotropy parameters were obtained by an adiabatic description, only taking into account the $e\,^3\Pi_g$ state. In this paper it is shown that inclusion of rovibronic couplings of the adiabatic $e\,^3\Pi_g$ state to the $k\,^3\Sigma_g^+$, $g\,^3\Sigma_g^+$, and $j\,^3\Delta_g$ Rydberg states not only improves the description of the resonances mentioned above, but also leads to new insights in photodissociation by barrier tunneling. The resonance width, the photofragment anisotropy, and the resonance intensity are all a strong function of electronic-state mixing and of coherent excitation of rotational resonances. The width of a resonance is affected by the coupling strength and character (bound versus quasibound) of the admixed state. The photofragment anisotropy is influenced upon mixing of dissociative continua. The cross section of a resonance is influenced not only by the transition moments of the admixed states but also by interference effects.

From earlier work [2–9] it is known that nonadiabatic couplings are very important for the $n=3$ Rydberg levels in H_2 below the $H(1s)+H(2l)$ dissociation limit to which the $e\,^3\Pi_g$ state belongs. Effects of these couplings on dissociation dynamics have been addressed in the work of Koot *et al.* [5]. For example, nonadiabatic coupling of the $j\,^3\Delta_g$ state with the $e\,^3\Pi_g$ state is responsible for the observation of fluorescence of the j-state levels to the repulsive $k\,^3\Sigma_u^+$ state.

The present investigation introduces couplings among continuum states and between a bound and a continuum

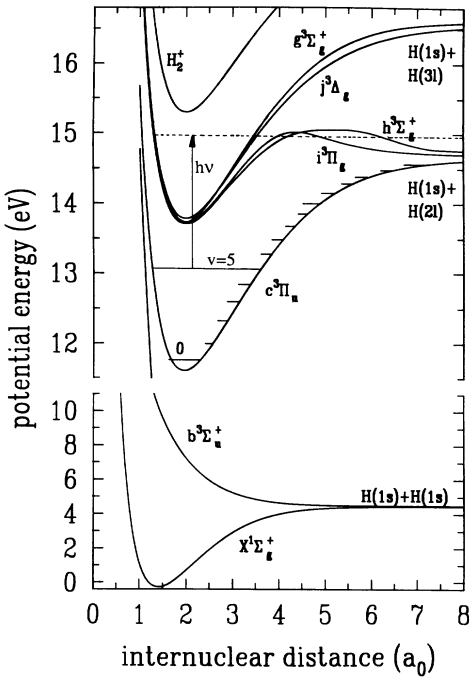

FIG. 1. Relevant adiabatic electronic potentials of H_2. Note the interchange of the labels between the two g and $k\,^3\Sigma_g^+$ state potential-energy curves with respect to Ref. [1] in accord with the recommendation of Ref. [7].

state in a formal treatment. The consequences of the couplings on the dynamics of photodissociation by barrier tunneling are discussed. The accuracy of the existing adiabatic potential-energy curves makes molecular hydrogen the ideal molecule to study the consequences of electronic-state mixing. However, all the effects studied pertain to excited molecular systems of both diatomic and polyatomic molecules.

In the experiments of Ref. [1], a fast beam of H_2 in several rovibrational levels of the metastable $c\,^3\Pi_u^-$ state is created by charge exchange of H_2^+ on Cs vapor. The metastable H_2 is dissociated by photon absorption around 600 nm. With our translational spectroscopy technique we determine simultaneously both the kinetic-energy release (KER) and the angle of dissociation with respect to the polarization vector of the laser. The observed KER value unambiguously determines the lower rovibrational level of the $c\,^3\Pi_u$ state. Recording the intensity of a peak in the KER spectrum as a function of the photon energy and the dissociation angle thus provides the relative differential photodissociation cross section of a specific rovibrational lower state. The experimental total cross sections and anisotropy parameters, already presented in Ref. [1], are given by the crosses in Figs. 2 and 3. The solid curves in these figures are the results from calculations to be discussed below. Inclusion of all couplings makes it possible to accurately calculate the differential photodissociation cross section spanning the complete (quasi-)continuum of the $n=3$ gerade manifold, in one calculation.

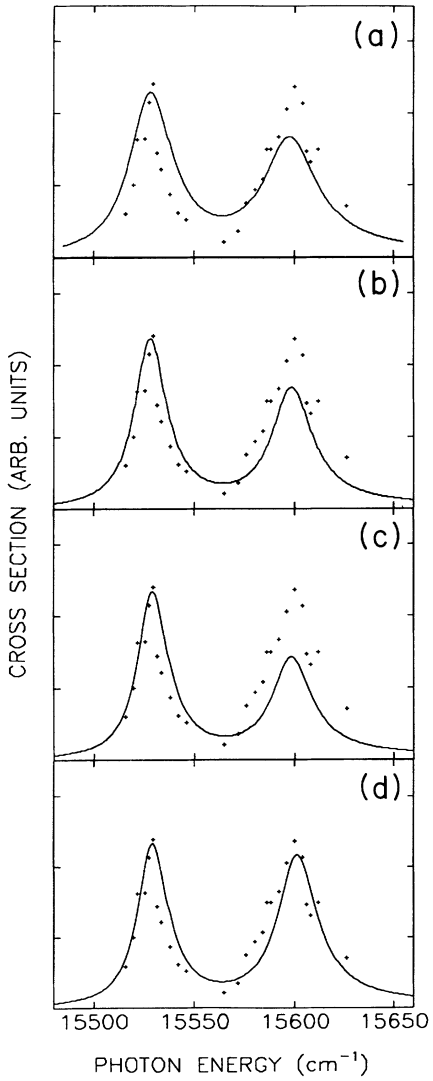

FIG. 2. Experimental and calculated total photodissociation cross sections. The experimental results are those from Ref. [1], the calculated results have been obtained by the methods discussed in the text.

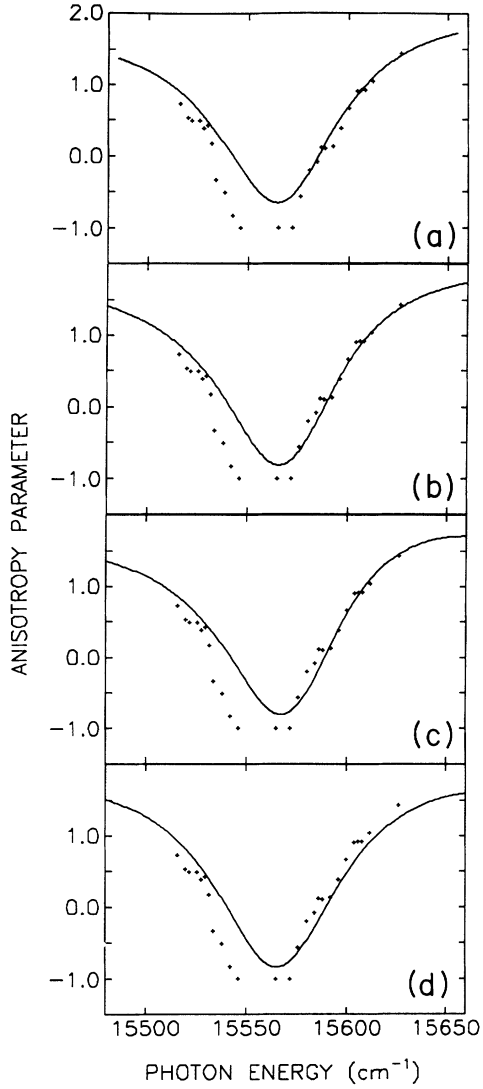

FIG. 3. Experimental and calculated anisotropy parameters. The experimental results are those from Ref. [1], the calculated results have been obtained by the methods discussed in the text.

II. THEORY

In this section a brief outline of the theory used to include all relevant states is presented. The nonrelativistic molecular Hamiltonian can be written as [7]

$$H=H_c+H' , \tag{1}$$

with H_c the clamped-nuclei (or Born-Oppenheimer) Hamiltonian and $H'=-1/2\mu\Delta_R$ the nuclear kinetic-energy operator. To calculate the photodissociation cross section of a molecule the molecular eigenfunctions Ψ_n, which fulfill the Schrödinger equation $H\Psi_n=E_n\Psi_n$, are needed [9]. The functions Ψ_n have definite spin multiplicity and electron inversion symmetry. Also, the total angular momentum exclusive of spin (N) is well defined. These functions can be written as a superposition of electronic-rotational wave functions ψ_i according to

$$\Psi_n=\sum_i \frac{1}{R}\psi_i(\mathbf{r};R,\phi,\theta)f_{in}(R) , \tag{2}$$

where $\mathbf{r}$ denotes the coordinates of all electrons, R is the internuclear distance, and the Euler angles θ and ϕ define the orientation of the internuclear axis. ψ_i are electronic-rotational wave functions with well-defined parity and can be written as

$$\psi_i=2^{\sigma}\left[\frac{2N+1}{8\pi}\right]^{1/2}\{\psi^i_{\Lambda}(\mathbf{r};R)[D^N_{M\Lambda}(\phi,\theta,0)]^* +p_i\psi^i_{-\Lambda}(\mathbf{r};R)[D^N_{M-\Lambda}(\phi,\theta,0)]^*\} , \tag{3}$$

with $\psi^i_{-\Lambda}(\mathbf{r};R)$ the electronic wave function, $[D^N_{M-\Lambda}(\phi,\theta,0)]^*$ a Wigner rotational wave function [10] describing the rotation of the molecule with M the projection of $\mathbf{N}$ on the laboratory Z axis, and Λ the component along the internuclear axis. p_i is the symmetry index [11], which is zero for Σ states with $\Lambda=0$, $\sigma=\frac{1}{2}$ for Σ states, and $\sigma=0$ otherwise. Substitution of Eq. (2) into Eq. (1) gives for a molecule with reduced mass μ a set of coupled equations in R only:

$$\left[-\frac{1}{2\mu}\left[\mathbf{I}\frac{d^2}{dR^2}+\mathbf{A}(R)+2\mathbf{B}(R)\frac{d}{dR}\right] +\mathbf{U}(R)-E\right]\mathbf{f}(R)=\mathbf{0} . \tag{4}$$

$\mathbf{I}$ is the identity matrix. The elements of the matrix $\mathbf{U}$ are given by

$$U_{ij}(R)=\langle\psi_i|H_c|\psi_j\rangle +\frac{1}{2\mu R^2}[N(N+1)+\langle\psi_i|\mathbf{L}^2|\psi_j\rangle-2\Lambda^2]\delta_{ij} , \tag{5}$$

with $\mathbf{L}$ the electronic angular momentum. The matrix $\mathbf{U}$ is diagonal if adiabatic electronic states are used in the wave functions ψ_i. The second term on the right-hand expression of Eq. (5) is the centrifugal potential [10], which only contributes to the diagonal elements of $\mathbf{U}$. Off-diagonal matrix elements of $\mathbf{L}^2$ are neglected in this treatment. The elements of the nonadiabatic coupling matrices $\mathbf{A}$ and $\mathbf{B}$ are given by

$$A_{ij}(R)=\left\langle\psi_i\left|\frac{d^2}{dR^2}\right|\psi_j\right\rangle -\frac{1}{2\mu R^2}\langle\psi_i|N_+L_-+N_-L_+|\psi_j\rangle , \tag{6}$$

$$B_{ij}(R)=\left\langle\psi_i\left|\frac{d}{dR}\right|\psi_j\right\rangle . \tag{7}$$

For large internuclear distances the coefficients for the open channels (i.e., for those electronic states $|\psi^i_{\Lambda}\rangle$ for which the energy E is in their vibrational continuum) the coefficients f_{in} are given by

$$f_{in}(R\rightarrow\infty)=a_{in}\sin(kR+\delta_{in}) , \tag{8}$$

while the coefficients of the closed channels vanish. The nuclear kinetic energy for the open channel is given by $\varepsilon=\hbar^2k^2/2\mu$ and δ_{in} is a phase shift. n_0 open channels give n_0 independent solutions at each energy of E of Eq. (4); the index n in Eq. (8) runs from 1 to n_0.

According to Ref. [9] the probability of the molecule being photodissociated into the solid angle $d\Omega=\sin\theta\,d\theta\,d\phi$ is equal to

$$\frac{d\sigma(\theta,\phi)}{d\Omega}\sim\sum_M\lim_{R\rightarrow\infty}\int||\Phi(t)\rangle|^2R^3d\mathbf{r} , \tag{9a}$$

where the integration is performed over the coordinates of all electrons, denoted by $\mathbf{r}$. For an isotropic initial state the summation over M is performed with equal weights and Eq. (9a) will be of the form

$$\frac{d\sigma(\theta,\phi)}{d\Omega}\sim\sigma_0[1+\beta P_2(\cos\Theta)] , \tag{9b}$$

with σ_0 is the total cross section, β the anisotropy parameter, and P_2 the second Legendre polynomial [10]. For large internuclear distance R the time-dependent wave function Φ is given by

$$\Phi(R\rightarrow\infty,t)=\sum_{N',M',i,n}A^i_{N'}(n)\psi_i\langle\Psi_n|H_{\rm int}|\Phi_0\rangle\frac{e^{ikR}}{R}e^{-iEt} , \tag{10a}$$

with

$$A^i_{N'}(n)=a_{in}\exp(i\delta_{in}) , \tag{10b}$$

the product of the amplitude and a factor containing the phase of the wave function in Eq. (8). $H_{\rm int}$ is the radiation-matter interaction Hamiltonian [12]. At this point it is important to note that the matrix element $\langle\Psi_n|H_{\rm int}|\Phi_0\rangle$ is a real number, the sign of which is determined by both the lower and upper states. This sign is thus not determined by the phase δ_{in} only.

Only the open channels, which contribute to the wave functions Ψ_n, contribute to the summation over i in Eq. (10), since the closed channels have zero amplitude for large R, i.e., $A^{i=\text{closed}}_{N'}(n)=0$. As a consequence the anisotropy parameter is dominated by the symmetry of the open channels. The differential photodissociation cross section can be calculated from Eqs. (9) and (10). In the

case of only one open channel $|A^{i}_{N'}(n)|$ is given by the energy normalization of the continuum wave function.

III. CALCULATIONS

The adiabatic $n=3$ gerade electronic Rydberg states are the $g\,^3\Sigma_g^+$, $k\,^3\Sigma_g^+$, $i\,^3\Pi_g$, and $f\,^3\Delta_g$ states; see Fig. 1. In the present work photodissociation of only one lower level is considered, namely the $v=5$, $N=1$ level in the $c\,^3\Pi_u^-$ state. In Ref. [1] photon excitation occurs around resonances identified spectroscopically as the $v'=5$, $N'=1$, and $N'=2$ quasibound $i\,^3\Pi_g$ states. Excitation involves a Q and an R transition, respectively. The summation over N' in Eq. (10) thus reduces to $N'=1$ and 2. Since linearly polarized light is considered, the summation over M' reduces to $M'=M$. Note that the Q and R transitions occur coherently according to Eq. (10).

The total angular momentum N' is conserved in intramolecular couplings. So those states reached by a Q transition are mutually coupled, as are those reached by an R transition. Selection rules [9] allow a Q transition to the coupled $N'=1$ $g\,^3\Sigma_g^+$ $k\,^3\Sigma_g^+$, and $i\,^3\Pi_g^+$ states. At the energy of interest the Q transition involves one closed (g) and two open (k,i^+) channels. The R transition occurs to the coupled $N'=2$ $i\,^3\Pi_g^-$ and $f\,^3\Delta_g^-$ states, of which the first is an open and the second a closed channel. Thus two sets of, respectively, three and two coupled states ought to be treated.

A. The Q transition

To obtain the coupled $N'=1$ $g\,^3\Sigma_g^+$, $k\,^3\Sigma_g^+$, and $i\,^3\Pi_g^+$ states Eq. (4) has to be solved. Numerically this equation simplifies, if $\mathbf{B}(R)=\mathbf{0}$, since then the first derivative in Eq. (4) disappears. The matrix $\mathbf{B}(R)$ contains large off-diagonal elements for the adiabatic $g\,^3\Sigma_g^+$ and the $k\,^3\Sigma_g^+$ states. A strongly avoided crossing [3] exists between the adiabatic potential curves of these states near the equilibrium nuclear separation as a consequence of this coupling. For the singlet manifold of molecular hydrogen Senn, Quadrelli, and Dressler [13] have described a transformation of the adiabatic electronic states to eliminate the nonadiabatic coupling matrix $\mathbf{B}(R)$. However, after this transformation the transformed matrix elements of $\mathbf{A}(R)$ are not known. Therefore we follow the semiempirical treatment given by Schins *et al.* [7], who looked for a minimum in the transformed matrices $\mathbf{A}(R)$ and $\mathbf{B}(R)$ that involved the $g\,^3\Sigma_g^+$ and the $k\,^3\Sigma_g^+$ states. As a criterion for the transformation, reproduction of the spectroscopic levels was used. This transformation removes the avoided crossing and yields diabatic states of nearly pure $|3s\rangle$ and $|3d\rangle$ electronic character, which cross near their equilibrium separation and are given by

$$|3s\rangle=\sin\Theta|g\rangle+\cos\Theta|k\rangle\ , \tag{11a}$$

$$|3d\rangle=\cos\Theta|g\rangle-\sin\Theta|k\rangle\ . \tag{11b}$$

The rotation angle $\Theta(R)$ depends on the internuclear distance and at a proper choice of $\Theta(R)$ small $\mathbf{A}$ and $\mathbf{B}$ matrix elements for the Σ states result [7]. The diabatic potentials U_{3s} and U_{3d}, which are the diagonal matrix elements of the matrix $\mathbf{U}$ in Eq. (4) for the diabatic states $|3s\rangle$ and $|3d\rangle$, are now obtained from the adiabatic potentials of the $g\,^3\Sigma_g^+$ and $k\,^3\Sigma_g^+$ states [14], U_g and U_k, respectively, according to

$$U_{3s}=\langle 3s|H_c|3s\rangle=U_g\sin^2\Theta+U_k\cos^2\Theta+U_{\mathrm{rot},3s}\ , \tag{12a}$$

$$U_{3d}=\langle 3d|H_c|3d\rangle=U_g\cos^2\Theta+U_k\sin^2\Theta+U_{\mathrm{rot},3d}\ . \tag{12b}$$

The centrifugal potentials are evaluated according to

$$U_{\mathrm{rot}}=[N'(N'+1)+L(L+1)-2\Lambda'^2]/2\mu R^2\ , \tag{13}$$

with a constant value of $L=0$ for the $|3s\rangle$ state and $L=2$ for the $|3d\rangle$ state, $N'=1$ and $\Lambda'=0$. The off-diagonal elements involving the diabatic Σ states follow from Eqs. (11) and are equal to

$$\langle 3s|H_c|3d\rangle=\tfrac{1}{2}(U_g-U_k)\sin 2\Theta\ . \tag{14}$$

The small but nonzero matrix elements in $\mathbf{A}(R)$ and $\mathbf{B}(R)$ that remain after the transformation are neglected in the present treatment. As a consequence the accuracy of Σ_g^+ level positions is limited to about 30 cm^{-1}.

The adiabatic potential of the $i\,^3\Pi_g$ state, $\langle i|H_c|i\rangle$, is provided by Kolos and Rychlewski [15]. The centrifugal potential, needed to evaluate the matrix element in $\mathbf{U}$ for the $i\,^3\Pi_g$ state, is calculated according to Eq. (13) with $L=2$, since the $i\,^3\Pi_g$ state has mainly $3d$ character around the equilibrium internuclear distance. The adiabatic corrections for the $i\,^3\Pi_g$ state, which appear in the matrix $\mathbf{A}$, have recently been calculated by Rychlewski [16] and are only different from zero near the top of the barrier.

The adiabatic Σ_g^+ states and the $i\,^3\Pi_g$ state are coupled by rotational coupling. A second advantage of diabatic Σ_g^+ states is that the L-uncoupling [10,17] matrix element given by the second term in Eq. (6) is almost zero between the $|3s\rangle$ and the $i\,^3\Pi_g$ ($3d$) electronic-rotational states. If this matrix element is neglected, the only nonzero off-diagonal elements in $\mathbf{A}$ are due to rotational coupling between the diabatic $|3d\rangle$ state and the adiabatic $i\,^3\Pi_g$ state. With a constant value of $L=2$ it is, for $N'=1$ according to the second term in Eq. (6), equal to $-\sqrt{12}/2\mu R^2$. The three coupled equations resulting from Eq. (4) for the $N'=1$ states reached by the Q transition can be solved numerically by using Eqs. (11)–(14) for the matrix elements. Table I provides a summary of these matrix elements and their origin.

B. The R transition

The $N'=2$ $i\,^3\Pi_g^-$ and $f\,^3\Delta_g^-$ states are coupled by the rotational motion only. All diagonal matrix elements in Eq. (4) involving the $i\,^3\Pi_g$ state have been introduced in Sec. III A. The adiabatic potential of the $f\,^3\Delta_g$ state have been given by Rychlewski [16]. No adiabatic corrections were available for the $f\,^3\Delta_g$ state. The centrifugal potentials have been evaluated according to the Eq. (13). The coupling due to the rotational motion is given by the second term in Eq. (6) and is equal to $-4/2\mu R^2$. Table I

TABLE I. Origin (reference or formula) of matrix elements of **A** and **U** in Eq. (4).

	ε'	$\mathscr{g}$	$3d$[a]	$3s$[a]
ε'	$\langle\varepsilon'\|H_c\|\varepsilon'\rangle$[b] $\langle\varepsilon'\|H'\|\varepsilon'\rangle$[d]	$\langle\varepsilon'^-\|H_{\rm rot}\|\mathscr{g}\rangle$[c]	$\langle\varepsilon'^+\|H_{\rm rot}\|3d^+\rangle$	
$\mathscr{g}$	$\frac{-4}{2mR^2}$	$\langle\mathscr{g}\|H_c\|\mathscr{g}\rangle$[e]		
$3d$	$\frac{-\sqrt{12}}{2mR^2}$		$\langle 3d\|H_c\|3d\rangle$[f]	$\langle 3s\|H_c\|3d\rangle$
$3s$			Eq. 14	$\langle 3s\|H_c\|3s\rangle$[h]

[a]Adiabatic Σ_g^+ state potentials $\langle\mathscr{g}|H_c|\mathscr{g}\rangle$ and $\langle\mathscr{h}|H_c|\mathscr{h}\rangle$ from Ref. [14], transformation $|\mathscr{g}\rangle,|\mathscr{h}\rangle\leftrightarrow|3d\rangle,|3s\rangle$ from Eqs. (11), and $\Theta(R)$ from Ref. [7].
[b]Rotational potential is added to the potential curves as in Eq. (13). Reference [15].
[c]The matrix is symmetric; upper right gives the matrix element, lower left the functional form or equation.
[d]Reference [16].
[e]Reference [18].
[f]Equation (12b).
[g]Equation (14).
[h]Equation (12a).

provides a summary of the matrix elements and their origin.

C. The differential photodissociation cross section

The coupled states $|\Psi_{n=1,2}\rangle$ for the two open channels with $N'=1$ and the state $|\Psi_{n=3}\rangle$ for the open channel with $N'=2$ and the coefficients $A^i_{N'}(n)$ have been obtained by solving the coupled equations described in Sec. III A and III B. With $i=3d$, ε'^-, and ε'^+ in Eq. (2) for respectively, the $|3d\rangle$, $\varepsilon'^3\Pi_g^+$, and $\varepsilon'^3\Pi_g^-$ states and

$$M_{N'}(n)=\langle\Psi_n|H_{\rm int}|\Phi_0\rangle\Big/\begin{bmatrix} N & 1 & N' \\ -M & 0 & M \end{bmatrix},$$

evaluation of Eqs. (9) and (10), using the properties of the Wigner functions and $3j$ coefficients [18] yields

$$\begin{aligned}\sigma_0\sim&[|A_1^{3d}(1)|^2+|A_1^{\varepsilon'^+}(1)|^2]|M_1(1)|^2\\&+[|A_1^{3d}(2)|^2+|A_1^{\varepsilon'^+}(2)|^2]|M_1(2)|^2\\&+\tfrac{5}{3}|A_2^{\varepsilon'^-}(3)|^2|M_2(3)|^2\end{aligned}\tag{15}$$

and

$$\begin{aligned}\beta=\{&[-|A_1^{3d}(1)|^2+\tfrac{1}{2}|A_1^{\varepsilon'^+}(1)|^2]|M_1(1)|^2+[-|A_1^{3d}(2)|^2+\tfrac{1}{2}|A_1^{\varepsilon'^+}(2)|^2]|M_1(2)|^2+\tfrac{5}{6}|A_2^{\varepsilon'^-}(3)|^2|M_2(3)|^2\\&+{\rm Re}[M_1(1)M_1(2)^*[-2A_1^{3d}(1)A_1^{3d}(2)^*+A_1^{\varepsilon'^+}(1)A_1^{\varepsilon'^+}(2)^*]\\&-\sqrt{15}[M_1(1)A_1^{\varepsilon'^+}(1)+M_1(2)A_1^{\varepsilon'^+}(2)]M_2(3)^*A_2^{\varepsilon'^-}(3)^*]\}/\{[|A_1^{3d}(1)|^2+|A_1^{\varepsilon'^+}(1)|^2]|M_1(1)|^2\\&+[|A_1^{3d}(2)|^2+|A_1^{\varepsilon'^+}(2)|^2]|M_1(2)|^2\\&+\tfrac{5}{3}|A_2^{\varepsilon'^-}(3)|^2|M_2(3)|^2\}\ .\end{aligned}\tag{16}$$

These (complicated) expressions are made more transparent in Sec. IV where the reduction of Eqs. (15) and (16) is given in the case of one-state calculations. In the total cross sections the three open channels can be recognized, of which the first two are two linear combinations of the $|3d\rangle$ and ε'^+ channels. Since all states above the H($2l$)+H($1s$) dissociation limit are now coupled to the dissociation continuum, the cross section of Eq. (15) describes not only the *dissociative* absorption cross section but the *total* absorption cross section. The matrix elements $M_{N'}(n)$ are sums of adiabatic transition matrix elements, which gives rise to strong intensity borrowing effects as will be shown later. The anisotropy parameter calculated in Eq. (16) contains the effects of interference most strongly through the last term in the numerator (Re$[M_1(1)\cdots]$) in which products between the strongly varying phase factors in $A^i_{N'}(n)$ give observable effects.

The cross sections and anisotropy parameters calculated according to Eqs. (15) and (16) are discussed in the following section. The electronic transition moments for excitation from the $c\,^3\Pi_u$ state to the adiabatic $n=3$ Rydberg state have been provided by Schins *et al.* [8]. Note that the dipole matrix elements for the diabatic $|3s\rangle$ and $|3d\rangle$ states are easily obtained from the adiabatic dipole moments for the $\mathscr{g}\,^3\Sigma_g^+$ and the $\mathscr{h}\,^3\Sigma_g^+$ states by using Eqs. (11).

IV. RESULTS AND DISCUSSION

A. Resonances due to $v'=5$, $N'=1,2$ in the $\varepsilon'^3\Pi_g$ state

To appreciate the importance of the various couplings discussed in Sec. III these are not all brought into account simultaneously. Exclusion of a state in the coupled equations can be performed by setting the relevant coupling matrix elements in Eq. (4) equal to zero and using a zero transition dipole moment in Eqs. (15) and (16) for the excluded state. The experimental results from Ref. [1] are presented together with several calculated results in Figs. 2 and 3. In Fig. 2 the relative total photodissociation cross sections are given. The calculated cross sections have been scaled such that the maxima of the experimental and calculated resonances at the lowest photon energy coincide. The anisotropy parameters are given in Fig. 3. The total cross section exhibits two resonances due to excitation to the quasibound $v'=5$, $N'=1$ and

$v'=5$, $N'=2$ $\epsilon'^3\Pi_g$ states, which are coupled to other $n=3$ Rydberg states. The anisotropy parameters in Fig. 3 are seen to vary drastically over the resonances, which is due to quantum interference. As has already been discussed in Ref. [1], coherent excitation of the $N'=1$ and 2 resonances in between the resonances gives $\beta=-1$, due to the fact that only one resonance has been passed, giving a phase shift difference of π [see Eq. (18) below].

Figure 2(a) contains the results presented previously [1]. The cross section has been calculated by use of the adiabatic potential of the $\epsilon'^3\Pi_g$ state [15], without bringing into account any nonadiabatic term. In this treatment only the continuum of the $\epsilon'^3\Pi_g$ state has to be taken into account and Eq. (16) reduces to

$$\beta=\frac{\frac{1}{2}|A_1^{\epsilon'^+}(1)|^2|M_1(1)|^2+\frac{5}{6}|A_2^{\epsilon'^-}(3)|^2|M_2(3)|^2+\mathrm{Re}\{-\sqrt{15}M_1(1)A_1^{\epsilon'^+}(1)[M_2(3)]^*A_2^{\epsilon'^-}(3)^*\}}{|A_1^{\epsilon'^+}(1)|^2|M_1(1)|^2+\frac{5}{3}|A_2^{\epsilon'^-}(3)|^2|M_2(3)|^2} . \tag{17}$$

The amplitudes $|A_1^{\epsilon'^+}(1)|=|A_2^{\epsilon'^-}(3)|$ are equal, due to the identical energy normalization of the continuum wave functions for $N'=1$ and 2. Only the phase factors in these $A_{N'}^{i}(n)$, given by $\exp(i\delta_{in})$, can be different. Equation (17) can now be written as

$$\beta=\frac{1}{2}+\frac{-\sqrt{15}M_1(1)M_2(3)\cos(\delta_{\epsilon'^+1}-\delta_{\epsilon'^-3})}{|M_1(1)|^2+\frac{5}{3}|M_2(3)|^2}$$

$$=\frac{1}{2}+\frac{3M_1M_2\cos(\delta_1-\delta_2)}{|M_1|^2+|M_2|^2} , \tag{18}$$

where the notation of Ref. [1] has been used in the second equality of Eq. (18). We note that this implies

$$M_{N'}(n)=M_{N'}\begin{bmatrix} N & 1 & N' \\ -\Lambda & 0 & \Lambda' \end{bmatrix}$$

for $n=1,3$ and $\Lambda=\Lambda'=1$, while $N=1$, $N'=1,2$, $\delta_1=\delta_{\epsilon'^+1}$ and $\delta_2=\delta_{\epsilon'^-3}$. The total cross section is proportional to $|M_1|^2+|M_2|^2$, a result already presented in Ref. [1]. The calculated curve in Fig. 2(a) has been shifted 15 cm^{-1} towards higher photon energy in order to let the positions of the calculated resonances coincide with the experimental ones. Apart from the discrepancy in the positions of the resonances, two other differences between the experimental and calculated results of Fig. 2(a) can be observed. The calculated widths of the resonances are larger than the experimental ones and the calculated intensity of the second resonance is too low. The calculated anisotropy parameters in Fig. 3(a) are in agreement with the experimental results around the second ($N'=2$) resonance at 15 600 cm^{-1}. However, around the first ($N'=1$) resonance and in between the two resonances the calculated anisotropy parameters are somewhat larger than the experimental results.

In Figs. 2(b) and 3(b) the calculated results have been obtained by inclusion of the adiabatic corrections [16] to the potential of the $\epsilon'^3\Pi_g$ state. The adiabatic corrections are given by the first term in the right-hand expression of Eq. (6). Inclusion of the adiabatic corrections makes the shift by 15 cm^{-1} superfluous and has narrowed the calculated resonances, resulting in a better agreement with the experimental total cross sections. The adiabatic corrections amount about 50 cm^{-1} on top of the barrier and vanish at other positions. Since the excitation takes place only 300 cm^{-1} below the top of the barrier, inclusion of these adiabatic corrections significantly decreases the tunneling probability. Nevertheless, the calculated intensity of the second resonance is still lower than observed experimentally. As is seen in Fig. 3(b), the calculated anisotropy parameters in between the two resonances are in somewhat better agreement with the experimental values. In this one-electronic-state description the numerator of the expression of β in Eq. (16) contains the real part of the product of the transition moments for excitation to $N'=1$ and 2 (see also Ref. [1]). This interference term is proportional to $\cos(\delta_1-\delta_2)$. Going over a resonance means a change of the corresponding phase δ_i by π resulting in a contribution of the interference term with opposite sign. The narrowing of the resonances gives rise to a faster change of the phase shifts $\delta_{N'}$ in the continuum wave functions of Eq. (8) as the photon energy is varied over the resonances. The anisotropy parameter thus exhibits larger changes as the resonances are more separated, since then the phase shift difference will get closer to π. However, around the first resonance the calculated anisotropy parameters are still larger than the experimental values.

Inclusion of the rotational coupling of the $\epsilon'^3\Pi_g^+(N'=1)$ state to the $g\,^3\Sigma_g^+(N'=1)$ and $k\,^3\Sigma_g^+(N'=1)$ states, with the Σ states mutually coupled vibrationally as discussed in Sec. III A, yields the results of Figs. 2(c) and 3(c). These results do not differ much from those of Figs. 2(b) and 3(b). The calculated resonance positions are not changed by the coupling with the Σ states. The width of the first calculated resonance in Fig. 2(c) is somewhat smaller than the corresponding width in Fig. 2(b). The reduction of the width reflects the larger bound character of the $N'=1$ wave function by inclusion of the Σ states. The increased bound character is mainly due to the barrier in the potential of the diabatic $(3d)\,^3\Sigma_g^+$ state, which is broader and higher than the barrier in the $\epsilon'^3\Pi_g$ state. Coupling with the purely bound diabatic $(3s)\,^3\Sigma_g^+$ state is hardly noticeable, since this state only mixes in indirectly via the $(3d)\,^3\Sigma_g^+$ diabatic state through the coupling of Eq. (14). The intensity of the second resonance has reduced somewhat in comparison to the results of Fig. 2(b). The smaller width of the first resonance gives rise to a smaller background below the second one. The calculated anisotropy parameters do not exhibit a significant change by inclusion of the Σ

states. This indicates that the outgoing flux via the Σ_g^+ continuum is small. Section IV B contains an example of a Σ dominated resonance in which the fluxes through the Σ_g^+ and the $\epsilon'^3\Pi_g^+$ continua are comparable.

Figures 2(d) and 3(d) contain the calculated results obtained by switching on the coupling with the $\gamma'^3\Delta_g^-$ state. All couplings considered in Sec. III are now brought into account. The agreement between the calculated and experimental cross section has improved dramatically. The calculated intensity of the second resonance has increased by about a factor of 1.5, bringing the calculated results in accord with the experimental findings. The large influence of the $\gamma'^3\Delta_g^-$ ($N'=2$) state initially came as a surprise and can be attributed to a number of effects.

First, there is the large effect of the rotational coupling of the quasibound $\epsilon'^3\Pi_g^-(v'=5, N'=2)$ state with the bound $\gamma'^3\Delta_g^-(v'=4, N'=2)$ state. It turns out that the $\gamma'^3\Delta_g^-(v'=4, N'=2)$ state is positioned only 490 cm^{-1} below the $\epsilon'^3\Pi_g^-(v'=6, N'=2)$ resonance. More importantly, the adiabatic vibrational wave functions have the same structure at internuclear distances up to about $2.5a_0$, as is shown in Fig. 4, resulting in a large value of the L-uncoupling matrix element. This is supported by the result of a test calculation in which the electronic potential of the $\gamma'^3\Delta_g$ state had been shifted $0.25a_0$ towards larger internuclear distances. Due to this shift the vibrational wave functions of the $\epsilon'^3\Pi_g^-(v'=5, N'=2)$ and the $\gamma'^3\Delta_g^-(v'=4, N'=2)$ state are almost orthogonal and the influence of the inclusion of the $\gamma'^3\Delta_g$ state in the calculations indeed disappeared. The $\epsilon'^3\Pi_g^-(v'=5, N'=2)$ resonance width decreased by about 10%, reflecting the increased bound character of the excited state.

Second, the large increase in the calculated intensity by about 50% is partly due to the large excitation probability of the $\gamma'^3\Delta_g$ state. The transition moment including the Hönl-London factor is about $\sqrt{2.5}$ times larger for excitation to the $\gamma'^3\Delta_g(N'=2)$ state than to the $\epsilon'^3\Pi_g(N'=2)$ state. Due to the fact that the total photodissociation cross section is determined by the square of the summed transition moments to the $\epsilon'^3\Pi_g$ and $\gamma'^3\Delta_g$

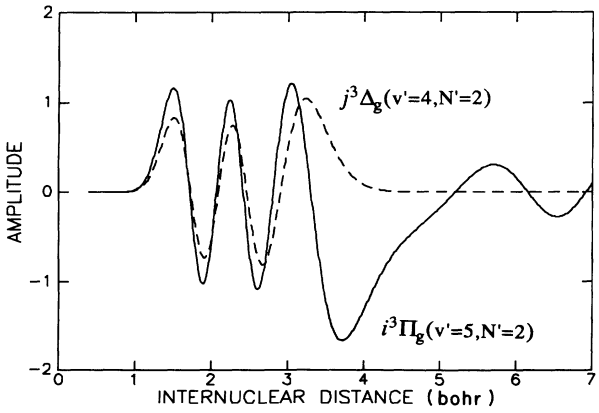

FIG. 4. Adiabatic vibrational wave functions of the $\epsilon'^3\Pi_g(v'=5, N'=2)$ state (solid curve) and the $\gamma'^3\Delta_g(v'=4, N'=2)$ state (dashed curve).

TABLE II. Calculated photon absorption cross section obtained without and with rotational couplings.

State	Cross section (arb. units) Without coupling	With coupling
$\gamma'(4,2)$	0.15	0.05
$\epsilon'(5,2)$	0.14	0.21
total	0.29	0.26

states, electronic state mixing can lead to large intensity shifts. For example, admixture of 10% of the γ' state gives, via the increased transition moment and the double product (from taking the square of a sum), a 50% effect on the absorption probability. The aspect of effective intensity borrowing in electronic state mixing is shown in Table II. The sum of the photon absorption cross sections calculated by bringing into account couplings should be equal to that obtained without couplings, since the couplings imply a unitary transformation of the states involved. The $\epsilon'^3\Pi_g^-(v'=5, N'=2)$ resonance is indeed mainly affected by the $\gamma'^3\Delta_g^-(v'=4, N'=2)$ state. Indeed, the sums of the absorption cross sections calculated without and with rotational coupling are within 10% the same. Note the admixture of ϵ'- state character to the γ' state ($v'=4$, $N'=2$) decreases the intensity of the latter resonance by a factor of 3.

The present case of coupling for $N'=2$ concerns the bound $\gamma'^3\Delta_g^-(v'=4, N'=2)$ state in the continuum of the $\epsilon'^3\Pi_g^-(N'=2)$ state. Since these two states are coupled and both carry oscillator strength from the lower state one might think of treating this system by a Fano formalism [19]. In such an approach the continuum is usually supposed to have no structure. This implies that the continuum nuclear wave functions and hence the coupling matrix elements are independent of energy. In this approximation the influence of the $\gamma'^3\Delta_g^-(v'=4, N'=2)$ resonance would be negligible near the $\epsilon'^3\Pi_g^-(v'=5, N'=2)$ resonance. The $\epsilon'^3\Pi_g^-(v'=5, N'=2)$ resonance is about 10^4 linewidths away from the $\gamma'^3\Delta_g^-(v'=4, N'=2)$ resonance. However, near the $\epsilon'^3\Pi_g^-(v'=5, N'=2)$ resonance the amplitude of its continuum nuclear wave function changes dramatically with energy and a treatment with constant coupling matrix elements is not valid. The $\epsilon'^3\Pi_g^-(v'=5, N'=2)$ wave function gets bound character and an estimate of the effect of coupling treating both states as bound is more reasonable.

Coupling to the $\gamma'^3\Delta_g^-(N'=2)$ state has only a small influence on the calculated anistropy parameters [Figs. 3(c) and 3(d)]. The calculated β values have become somewhat smaller around the second resonance. The experimental error in the experimental β values does not allow us to decide if the calculated results of Fig. 3(d) are better than those discussed above.

B. Effects of nonadiabatic couplings on anisotropy of photofragmentation by barrier tunneling

In Sec. IV A is shown how the experimental differential photodissociation cross section is well described by in-

clusion of nonadiabatic couplings. Rotational coupling of the $\epsilon\,^3\Pi_g^-(N'=2)$ state to the $\jmath\,^3\Delta_g^-(N'=2)$ state causes the total cross section to change dramatically. In this section a number of physical phenomena concerning coherence effects in the photodissociation by barrier tunneling in H_2 is illustrated. Again photodissociation of the $c\,^3\Pi_u^-(v=5,\ N=1)$ state suffices to illustrate these effects.

In Fig. 5 the photodissociation cross section and the anisotropy parameters calculated are presented. Figure 5 shows two resonances at 14 906 and 15 110 cm^{-1} with a very small width, which are due to excitation of the $\hbar\,^3\Sigma_g^+(v'=5\ N'=1)$ state and the $\jmath\,^3\Delta_g^-(v'=4,\ N'=2)$ state, respectively. The $\hbar$-state resonance energy is 29 cm^{-1} below the experimental value [4]. The spectroscopic use of the $\hbar$ and g-state label is not unambiguous. In Ref. [4] this resonance is described as $g\,^3\Sigma_g^+(v'=5,\ N'=1)$ resonance. The discrepancy in the calculated position is attributed to ignoring the remaining vibrational interactions between the (not perfect) diabatic Σ states (see Sec. III A) [20]. The resonant energy for excitation to the $\jmath\,^3\Delta_g^-(v'=4,\ N'=2)$ state is in perfect agreement with the experimental value [4].

If the $\hbar\,^3\Sigma_g^+$ state would be a pure Σ state, the photofragment anisotropy parameter would be equal to $\beta=-1$. The fact that the calculated anisotropy parameter on top of the $\hbar\,^3\Sigma_g^+(v'=5,\ N'=1)$ resonance is 0.1 indicates that the rotational coupling of this state with the $\epsilon\,^3\Pi_g^+$ state results in a reasonable outgoing flux through the barrier of the $\epsilon\,^3\Pi_g$ state. Koot *et al.* [5] have measured for this resonance an anisotropy parameter of $\beta=0.22$, close to the value calculated here. These authors already recognized that the flux through the barrier of the $\epsilon\,^3\Pi_g^+$ state must be considerable for this resonance [5]. Albeit that the coupling with the $\epsilon\,^3\Pi_g^+$ state is weak,

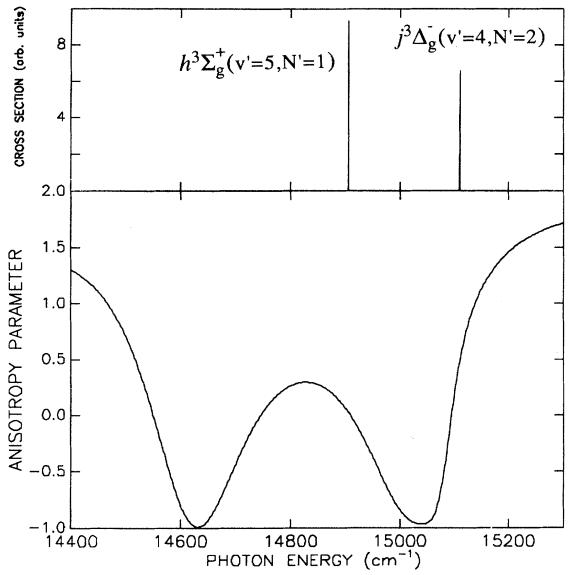

FIG. 5. Calculated cross sections (upper figure) and anisotropy parameters (lower figure) as discussed in the text. The peaks in the upper figure are due to the $\hbar\,^3\Sigma_g^+(v'=5,\ N'=1)$ and the $\jmath\,^3\Delta_g^-(v'=4,\ N'=2)$ resonances.

tunneling through the barrier of the $\epsilon\,^3\Pi_g$ state is much faster than through the (broad) barrier of the $\hbar\,^3\Sigma_g^+$ state. The coefficients $A^i_{N'}(n)$ show that the calculated flux through the $\epsilon\,^3\Pi_g$ channel is twice the flux through the $\hbar\,^3\Sigma_g^+$ state. Indeed, this ratio of the fluxes explains the calculated anisotropy parameter to be close to zero; the β parameters are 0.5 and -1 for dissociation by a pure Π_g^+ and Σ_g^+ continuum, respectively.

Another feature in Fig. 5 is worth mentioning, namely the change in the anisotropy parameter around the resonance at 15 110 cm^{-1}. We conclude that this is due to interference between direct excitation to the continuum of the $\epsilon\,^3\Pi_g$ state and dissociation by excitation to the $\jmath\,^3\Delta_g^-$ state, which is predissociative due to rotational coupling to the $\epsilon\,^3\Pi_g$ state. Fano profiles of this type are discussed in Ref. [17]. The $\jmath\,^3\Delta_g(v'=4,\ N'=2)$ resonance influences the anisotropy parameter over a much longer energy range than its linewidth. Apparently the amplitude of the $\epsilon\,^3\Pi_g$ quasicontinuum wave functions has become very small at 1000 cm^{-1} below the barriers and in between the $\epsilon\,^3\Pi_g(v'=4)$ and $(v'=5)$ resonances. Only at a relatively large energy distance of 70 cm^{-1} at 15 020 cm^{-1} the excitation probability to reach the $\jmath\,^3\Delta_g^-$ has decreased enough to make it comparable to that for excitation to the $\epsilon\,^3\Pi_g$ state and give rise to maximum interference.

Finally, in Fig. 5 the anisotropy parameter is also seen to change around a photon energy of 14 600 cm^{-1}, while there is *no resonance being observed.* Since there is no resonance at this photon energy no rapidly varying phase δ_i is present, as is the case in between the rotational resonances described in Sec. IV A. Only the $\epsilon\,^3\Pi_g$ state needs to be considered near 14 600 cm^{-1} because no $\hbar\,^3\Sigma_g^+$ state resonances occur near this energy. In between the $v'=4$ and 5 resonances of the $\epsilon\,^3\Pi_g$ state the phase shifts δ_1 and δ_2 change smoothly with energy and are almost equal, yielding $\cos(\delta_1-\delta_2)\approx 1$ [Eq. (18)]. The observed change of the anisotropy parameter coincides with a minimum of the total cross section in the upper panel of Fig. 5, and is caused by a change of the sign of the matrix elements M_1 and M_2 in Eq. (18). In the considered energy region the vibrational quasicontinuum wave function goes from a $v'=4$ to a $v'=5$-like resonance, and as a consequence the transition moments M_1 and M_2 change sign. The change occurs at a somewhat lower energy for $N'=1$ than for $N'=2$. The matrix element M_1 equals zero for a photon energy near 14 530 cm^{-1}, giving $\beta=0.5$ [Eq. (18)]. Above this energy excitation to $N'=1$ takes place to the low-energy side of the $v'=5$ resonance, while excitation to $N'=2$ still involves the high-energy side of the $v'=4$ classical values again; see Eq. (18). If $M_1=-M_2$, β becomes $\beta=-1$. It should be stressed that the magnitudes and signs of these transition moments are determined by the wave function of the lower $c\,^3\Pi_u^-(v'=5,\ N'=1)$ state. Therefore it is concluded that this change in the photofragment anisotropy has no parallel in an atom-atom collision where only the excited state is of importance. At 14 600 cm^{-1} M_2 changes sign. From here both branches reach a $v'=5$ resonance and the anisotropy parameter goes up. The presence of the

$k\,^3\Sigma_g^+(v'=5,\ N'=1)$ resonance prevents β to become larger than about 0.4.

It should be noted that the described change of the anisotropy parameter will be extremely hard to observe, since at this position in the quasicontinuum the cross section displays a minimum.

V. CONCLUSIONS

This paper has been inspired by discrepancies between a one-state calculation and the experimental result on the photodissociation of H_2 through the barrier of the $i\,^3\Pi_g$ state. However, this work has provided insights in the consequences of electronic mixing through rotational and vibrational coupling on the dynamics of dissociation through a potential barrier. The effects on the dynamics are observed by the shape and intensity of absorption resonances and by the change of the anisotropy parameter. In the $n=3$ system of H_2 two bound states, the $j\,^3\Delta_g$ and $(3s)g\,^3\Sigma_g^+$ and one quasibound state with a broad barrier, the $(3d)k\,^3\Sigma_g^+$ state, are mixed in.

The $k\,^3\Sigma_g^+(v'=5,\ N'=1)$ resonance forms an example where electronic mixing causes the excited molecules to dissociate in nearly equal amounts through the i-state barrier and k-state barrier as shown by the anisotropy parameter. Excitation in between the $v'=4$ and 5 resonance of the i state forms an example of coherent excitation of the $v'=5$, $N'=1$ and $v'=4$, $N'=2$ resonances. The change of sign of the Franck-Condon factor between $v'=4$ and 5 causes the occurence of nonclassical anisotropy parameters. This change in β parameter has no parallel in an atomic-collision problem. In contrast, the coherent excitation of the rotational levels $i\,^3\Pi_g(v'=5,\ N'=1$ and $v'=5,\ N'=2)$ also results in nonclassical β parameters now due to phase changes of the continuum wave functions over the resonances.

The last example has been confronted with the experimental observations. Subsequently, different nonadiabatic effects have been incorporated. Adiabatic corrections to the potential of the $i\,^3\Pi_g$ state improve the calculated resonance widths, resonance positions, and anisotropy parameters. Rotational coupling of the $i\,^3\Pi_g^+(N'=1)$ state to the mutually vibrationally coupled $g\,^3\Sigma_g^+(N'=1)$ and $k\,^3\Sigma_g^+(N'=1)$ states does not have a significant effect on the calculated results. Rotational coupling of the $i\,^3\Pi_g^-(N'=2)$ state with the $j\,^3\Delta_g^-(N'=2)$ greatly enhances the agreement between theory and experiment. The coupling with the $j\,^3\Delta_g^-(N'=2)$ state increases the relative intensity of the $N'=2$ resonance by 50% and brings it into agreement with the experimental results.

ACKNOWLEDGMENTS

Dr. J. Los and Dr. H. G. Muller are gratefully acknowledged for the useful discussions. This work is part of the research program of the Stichting voor Fundamenteel Onderzoek der Materie (Foundation for the Fundamental Research on Matter) and was made possible by the financial support of the Nederlandse Organisatie voor Wetenschappelijk Onderzoek (Netherlands Organization for the Advancement of Research).

[1] L. D. A. Siebbeles, J. M. Schins, J. Los, and M. Glass-Maujean, Phys. Rev. A **44**, 343 (1991).
[2] M. L. Ginter, J. Chem. Phys. **46**, 3687 (1967).
[3] C. B. Wakefield and E. R. Davidson, J. Chem. Phys. **43**, 834 (1965).
[4] W. Koot, J. J. van der Zande, J. Los, S. R. Keiding, and N. Bjerre, Phys. Rev. A **39**, 590 (1989).
[5] W. Koot, P. H. P. Post, W. J. van der Zande, and J. Los, Z. Phys. D **10**, 233 (1988).
[6] S. R. Keiding and N. Bjerre, J. Chem. Phys. **87**, 3321 (1987).
[7] J. M. Schins, L. D. A. Siebbeles, J. Los, and W. J. van der Zande, Phys. Rev. A **44**, 4162 (1991).
[8] J. M. Schins, L. D. A. Siebbeles, W. J. van der Zande, J. Los, H. Koch, and J. Rychlewski, Phys. Rev. A **44**, 4171 (1991).
[9] L. D. A. Siebbeles, J. M. Schins, W. J. van der Zande, and J. A. Beswick, Chem. Phys. Lett. **187**, 633 (1991).
[10] R. N. Zare, *Angular Momentum* (Wiley, New York, 1988).
[11] M. H. Alexander and P. J. Dagdigian, J. Chem. Phys. **80**, 4325 (1984).
[12] R. Loudon, *The Quantum Theory of Light* (Clarendon, Oxford, 1973), Chap. 11.
[13] P. Senn, P. Quadrelli, and K. Dressler, J. Chem. Phys. **89**, 7401 (1988).
[14] W. Kolos and J. Rychlewski, J. Mol. Spectrosc. **143**, 212 (1990).
[15] W. Kolos and J. Rychlewski, J. Mol. Spectrosc. **66**, 428 (1977).
[16] According to J. Rychlewski (private communication), the $i\,^3\Pi_g$ potential must be increased by 56 cm^{-1} for $R=4.0$ bohr, 42 cm^{-1} for $R=5.0$ bohr, 1.5 cm^{-1} for $R=6.0$ bohr, and 0.1 cm^{-1} for $R=8.0$ bohr.
[17] L. D. A. Siebbeles, J. M. Schins, J. Los, and M. Glass-Maujean, Phys. Rev. A **44**, 1584 (1991).
[18] M. Rotenberg, R. Bivins, N. Metropolis, and J. K. Wooten, Jr., *The 3j and 6j Symbols* (MIT Press, Cambridge, 1955).
[19] U. Fano, Phys. Rev. **124**, 1866 (1961).
[20] J. M. Schins, L. D. A. Siebbeles, W. J. van der Zande, and J. Los, Chem. Phys. Lett. **182**, 69 (1991).